



Wavefront Sensing and Control Technology for Submillimeter and Far Infrared Space Telescopes

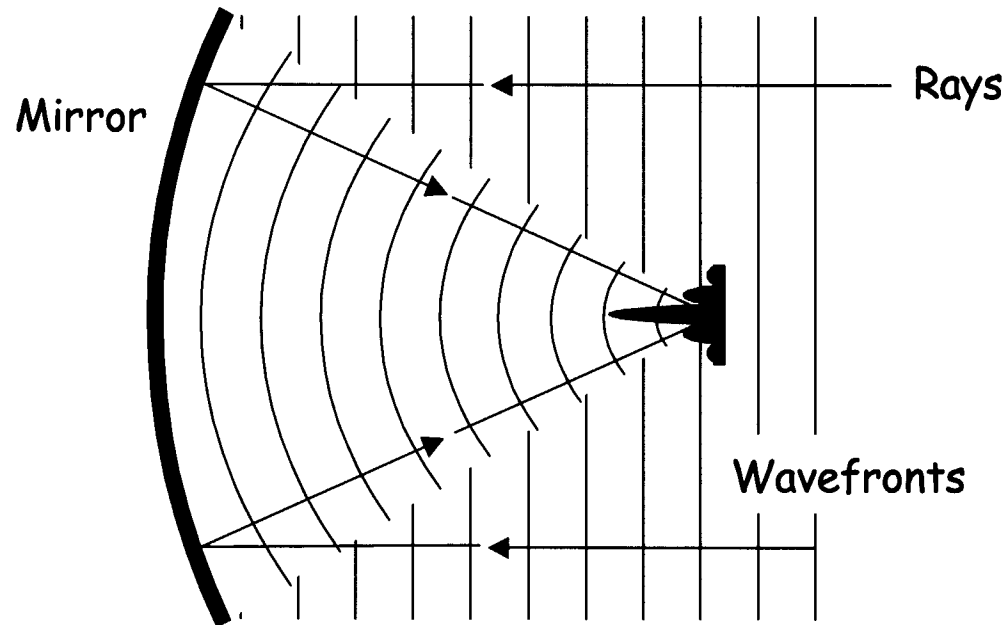
March 7-8, 2002

Dave Redding

Acknowledgements

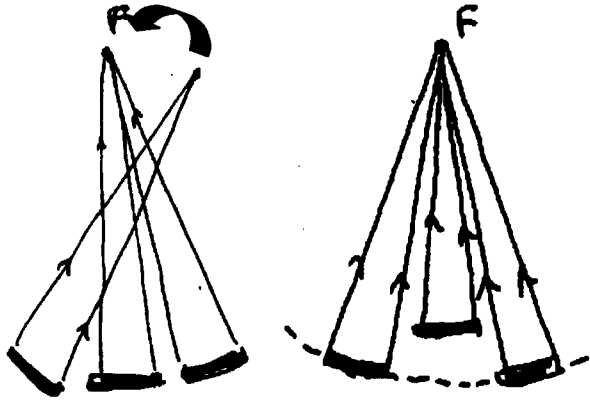
- NGST WFC Government Team:
 - At JPL: Scott Basinger, David Cohen, Phil Dumont, Joe Green, Andrew Lowman, Cathy Ohara, David Redding, Fang Shi, David Van Buren
 - At GSFC: Chuck Bowers, Laura Burns, Pam Davila, Bruce Dean, Peter Dogota, Kong Ha, Bill Hayden, Frank Liu, Gary Mosier, Peter Petrone, Gary Welter
- PSR, SMMM:
 - Eri Cohen, Ken Lau, David Redding, George Sevaston, Sam Sirlin
- SIM:
 - Mike Shao, Feng Zhao

Imaging and Wavefront Control



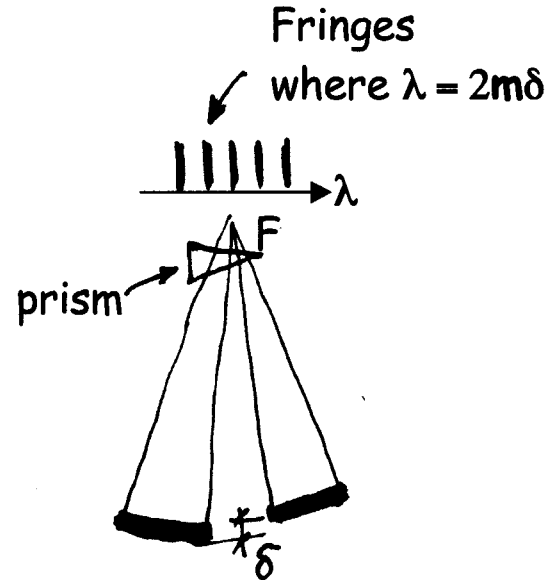
- A perfect optical system converts incoming wavefronts to concentric spherical wavefronts converging to a point image on a detector
- Imperfections arise from fabrication error, temperature changes, alignment shifts, strain relief, long-term dimensional change
 - Traditionally minimized using massive structures
- Wavefront control uses moving and deforming elements to compensate imperfections after launch
 - Replaces massive structures with computers and actuators

Principle of the wavefront control approach for NGST



1. COALIGNMENT AND COFOCUSING

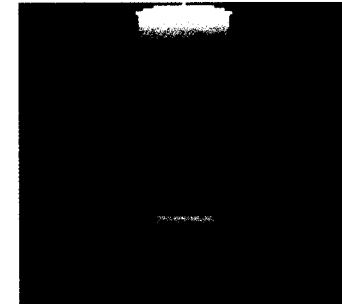
- Aligned to the accuracy of a single element telescope.
- Primary mirror piston $\sim 5\lambda$ (10 microns) (limited by depth of focus of individual segment)



2. COARSE PHASING

Dispersed fringe sensing

$$\text{WF error} < \lambda$$

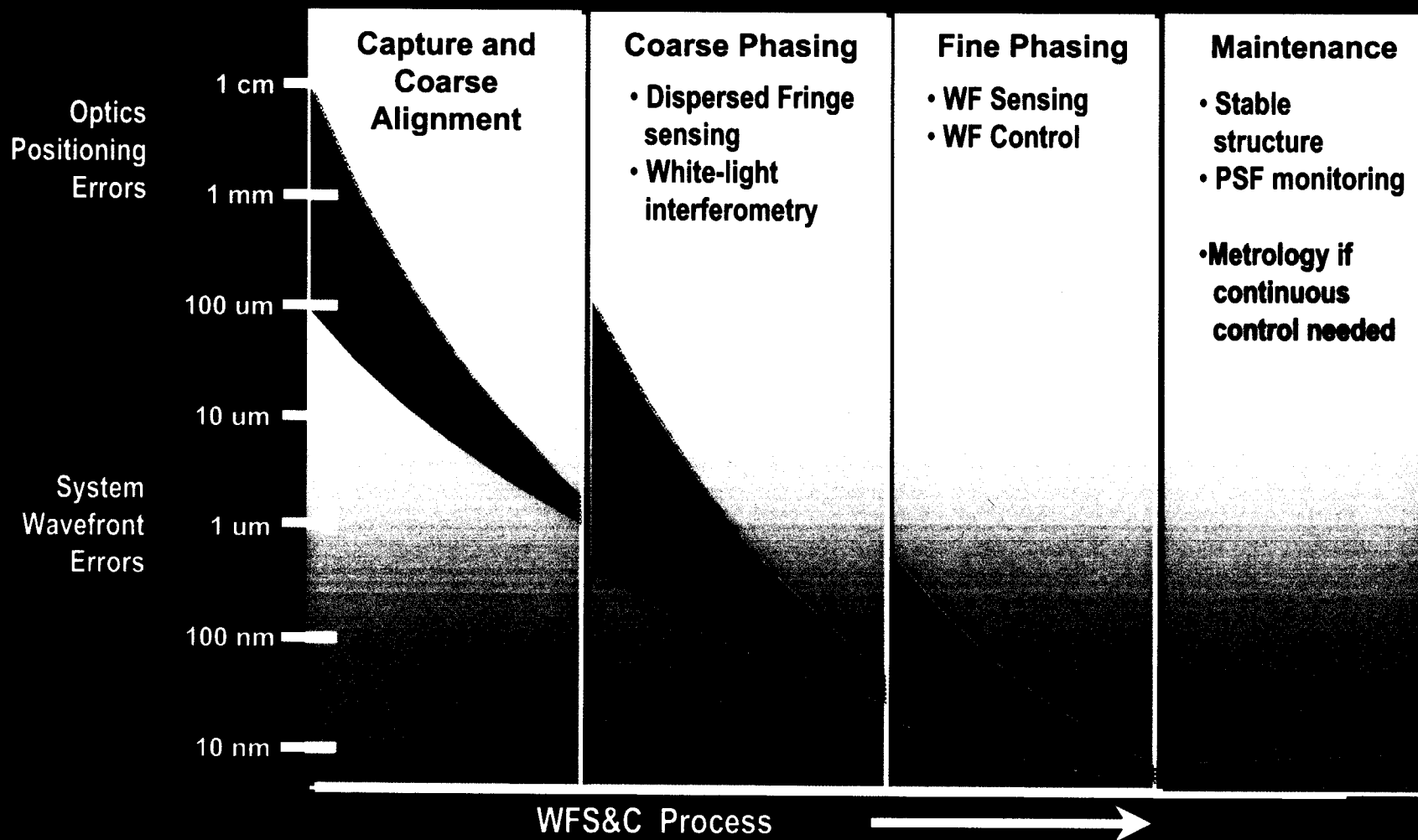


3. FINE PHASING

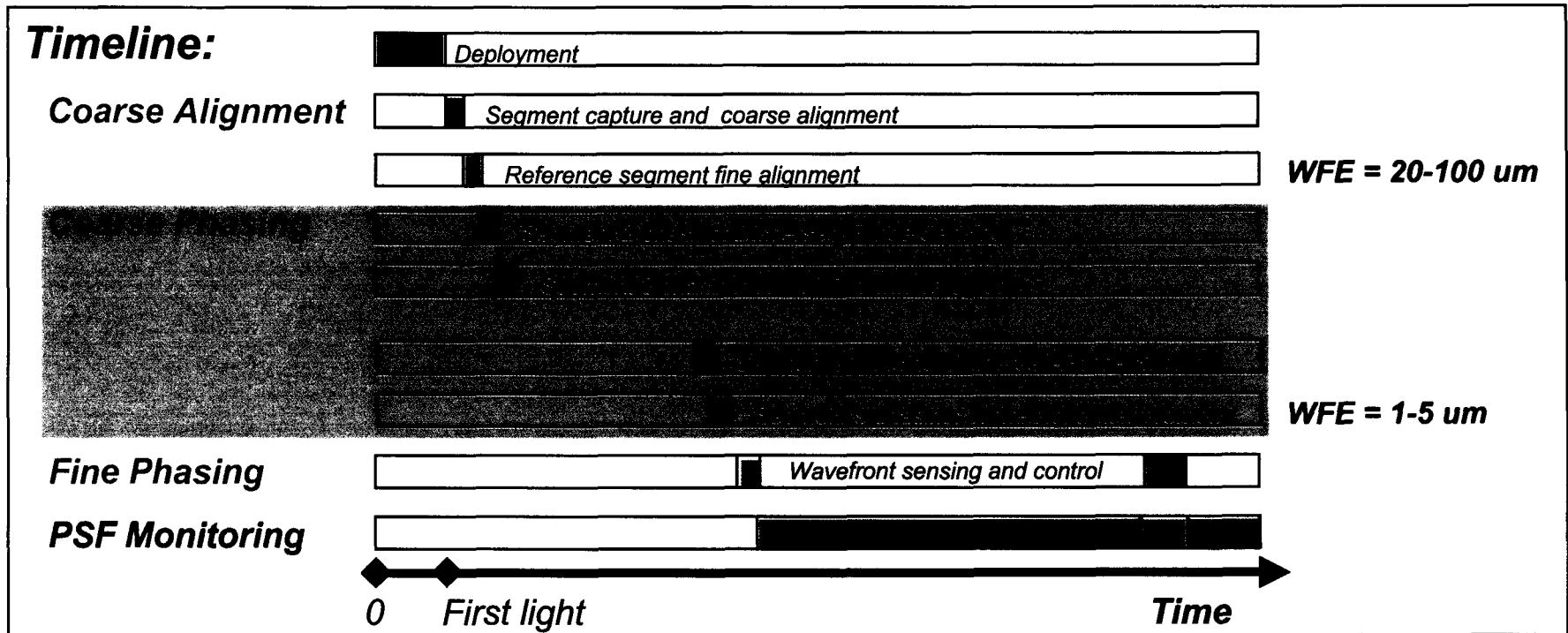
Phase retrieval

- WF measurement error $< \lambda/100$
- WF control error $< \lambda/20$

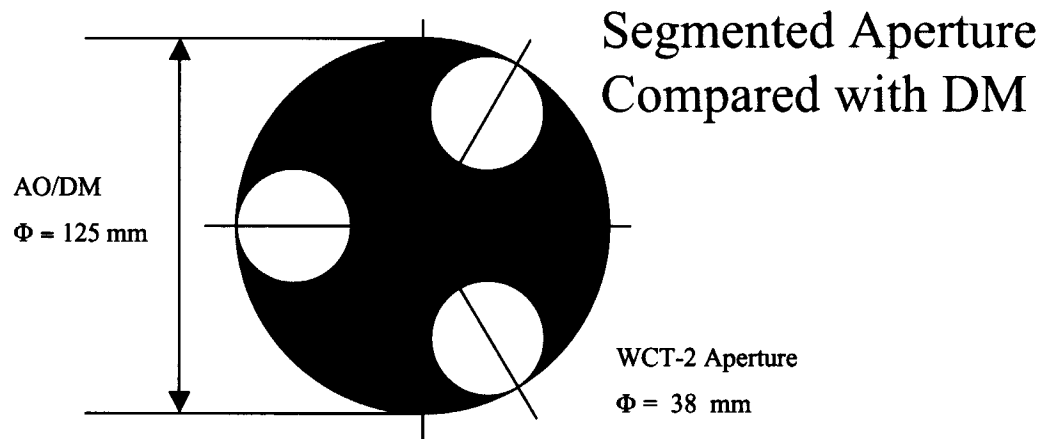
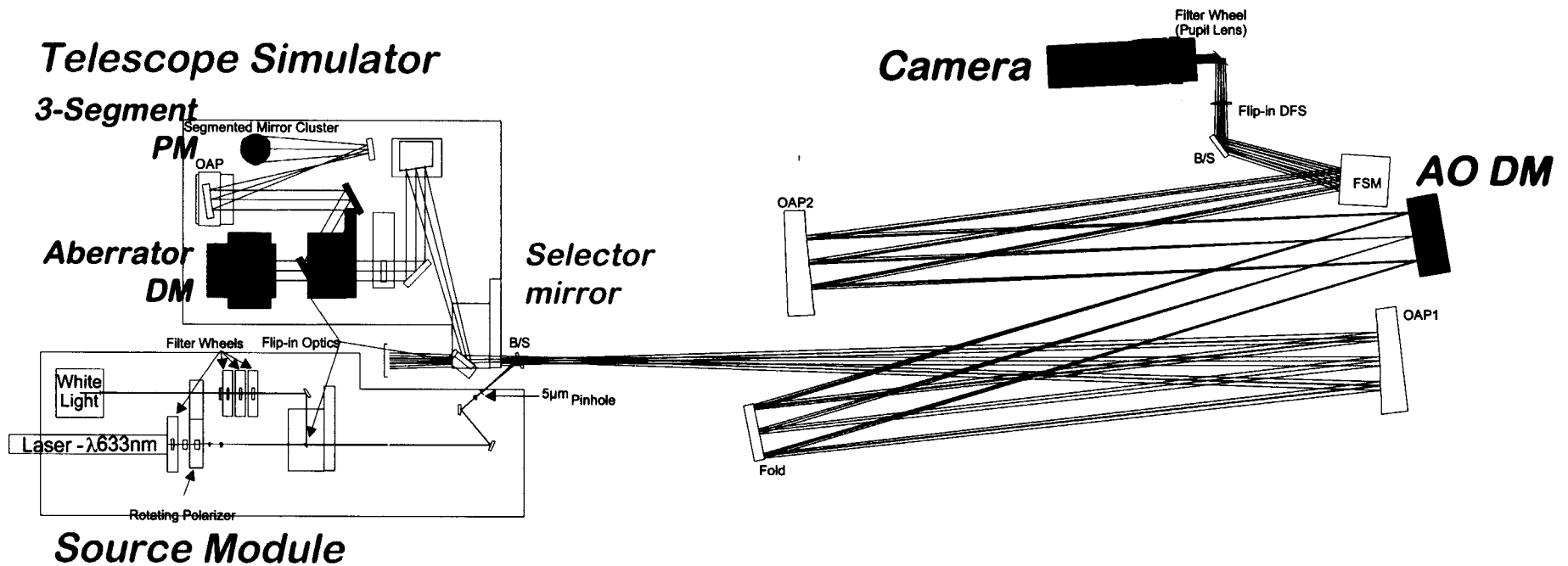
Wavefront Improvement During WFS&C



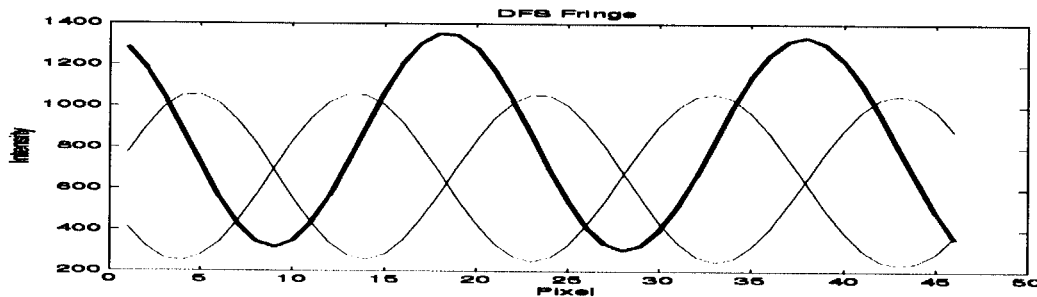
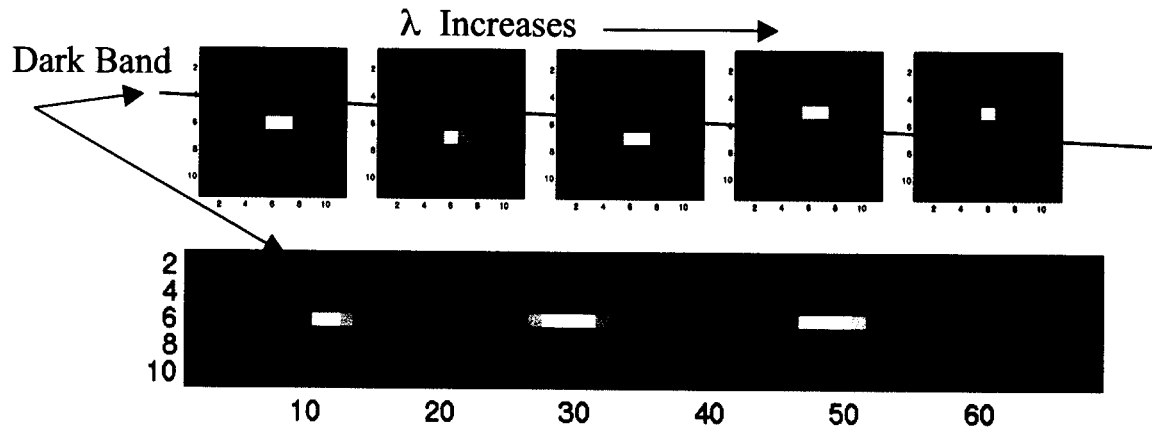
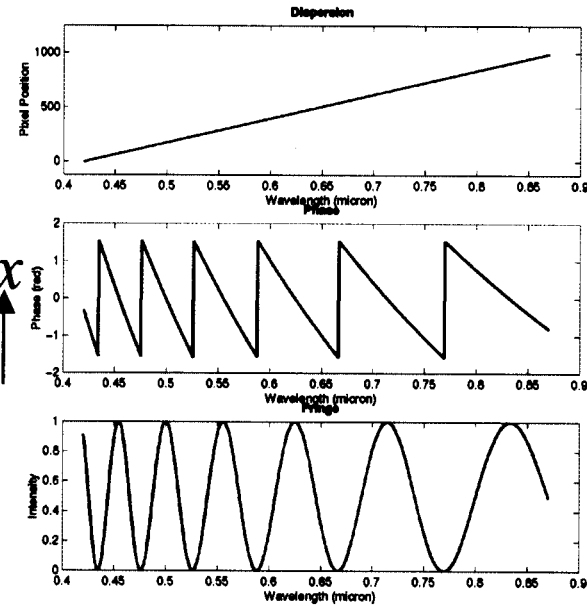
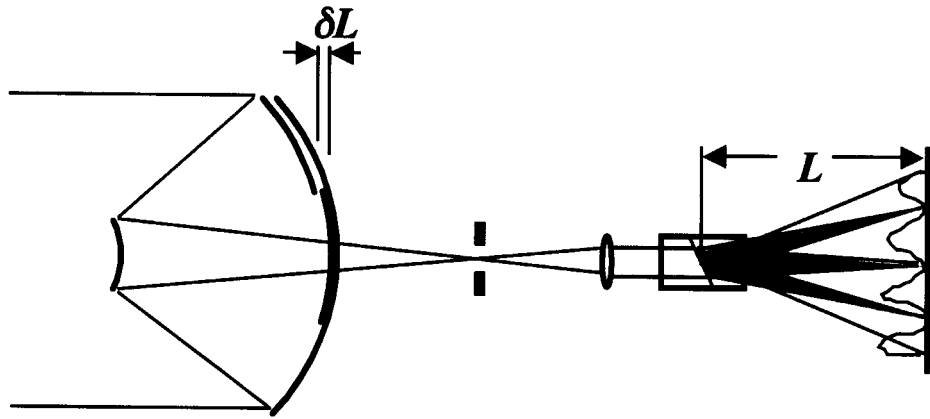
Coarse Phasing



WCT-2 Testbed Layout

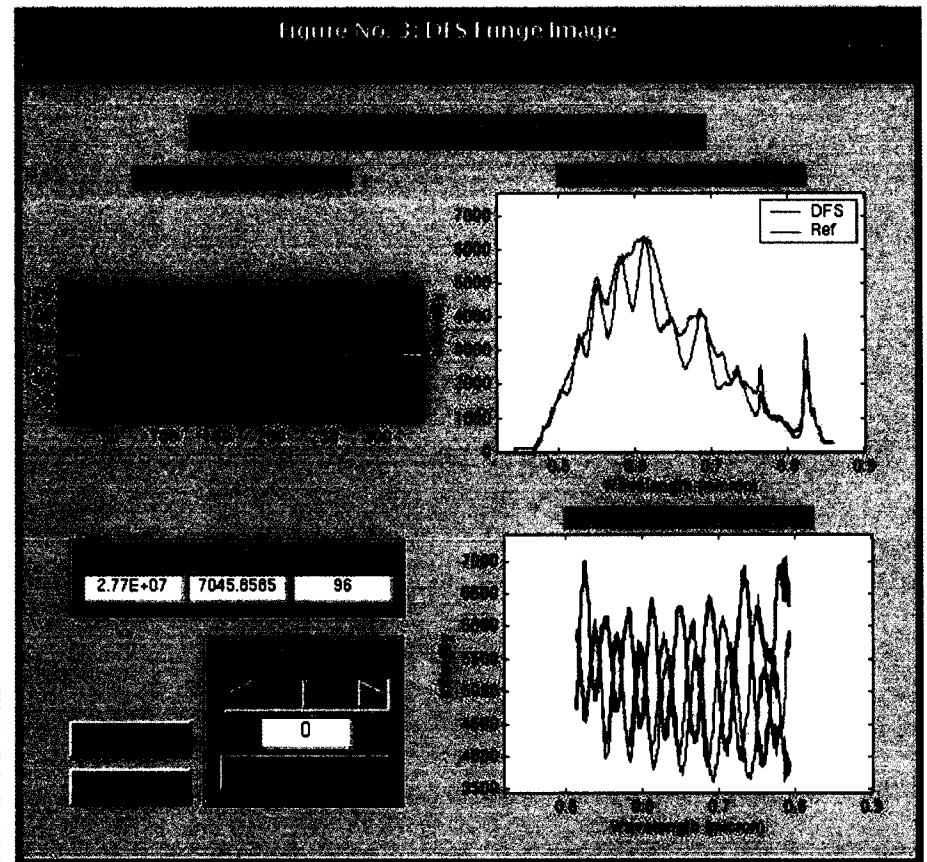
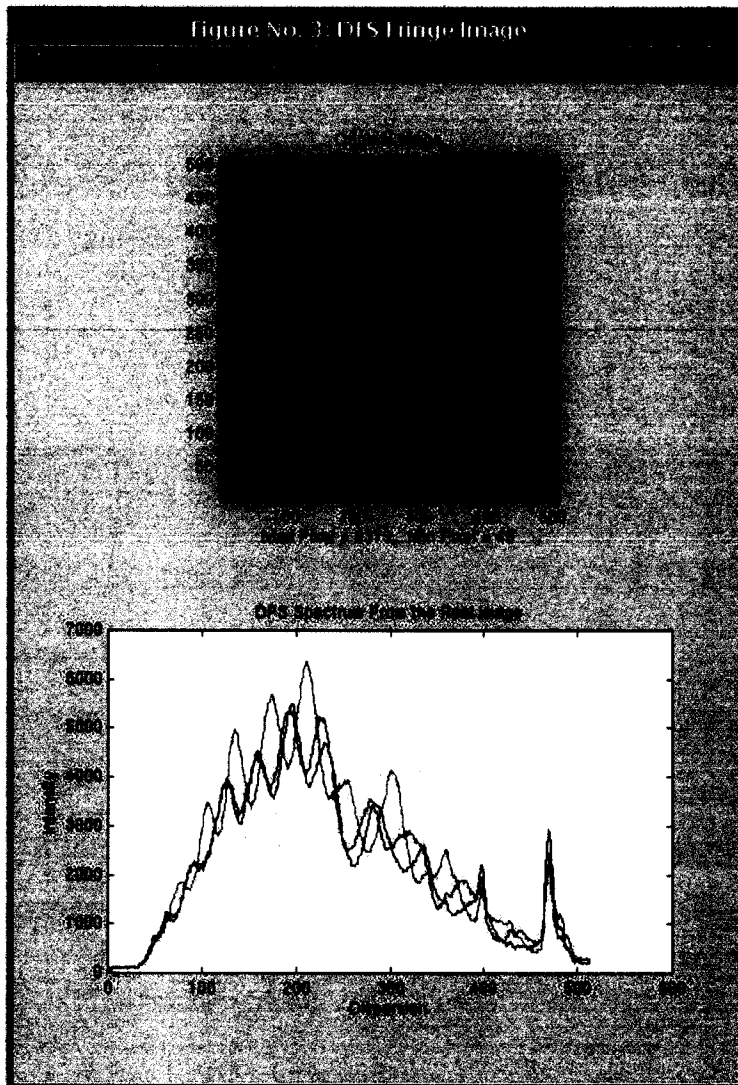


Dispersed Fringe Sensor (DFS)



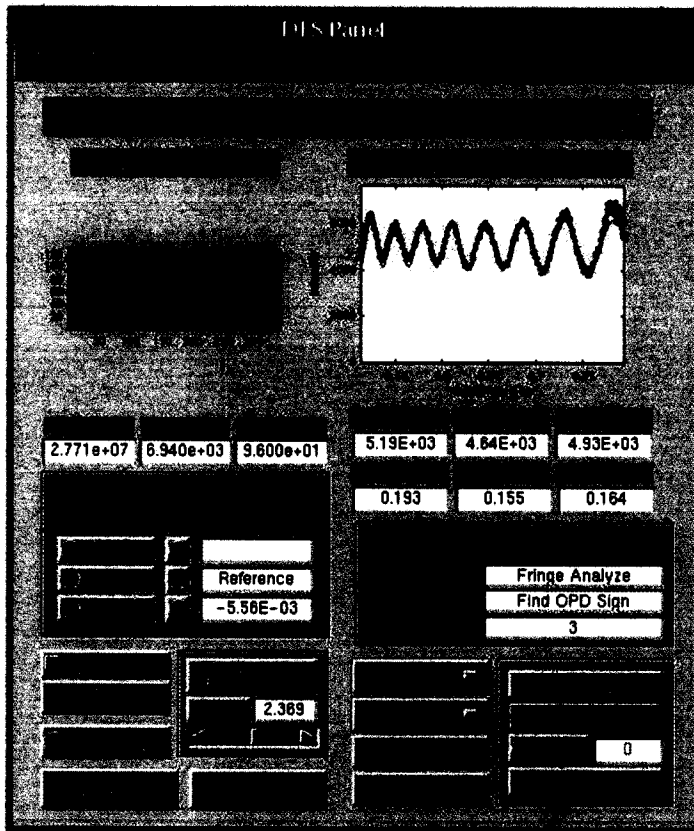
- DFS Modeled Fringe: DCATT Model
- Wavelength range: $\lambda = 624.8 - 658.8$ nm
- Piston error: $\delta L = 7 \mu\text{m}$

WCT-2 Demo: Fringe Pre-Processing (Segs #2 & #3)



- Panels displayed during data taking
- Left panel shows the raw DFS image and signals
- Right panel shows the removal of lamp spectrum

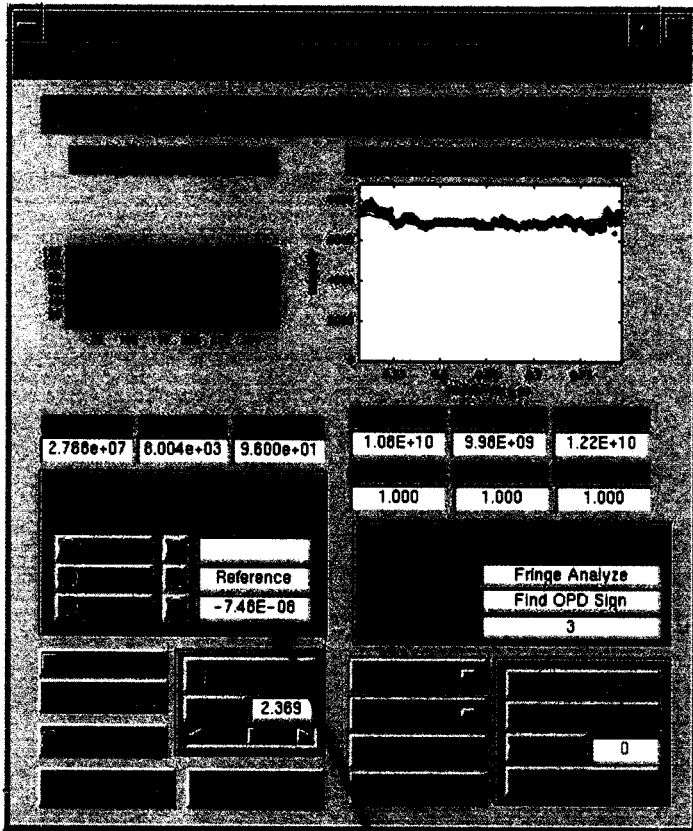
WCT-2 Demo: DFS Analysis (Segs #2 & #3)



- Processed DFS image (Seg #1 tilted out)
- Processed DFS fringe from Seg #2 and #3 (dotted lines).
- DFS fitted curve (solid lines)
 - Fringe period determines piston magnitude
 - Relative phase between sidelobe traces determines the sign (up or down) of the piston
 - DFS analysis result:
Relative Seg #3 Piston = -5.56 μm

Push here to implement piston correction

WCT-2 Demo: After Correction (Segs #2 & #3)

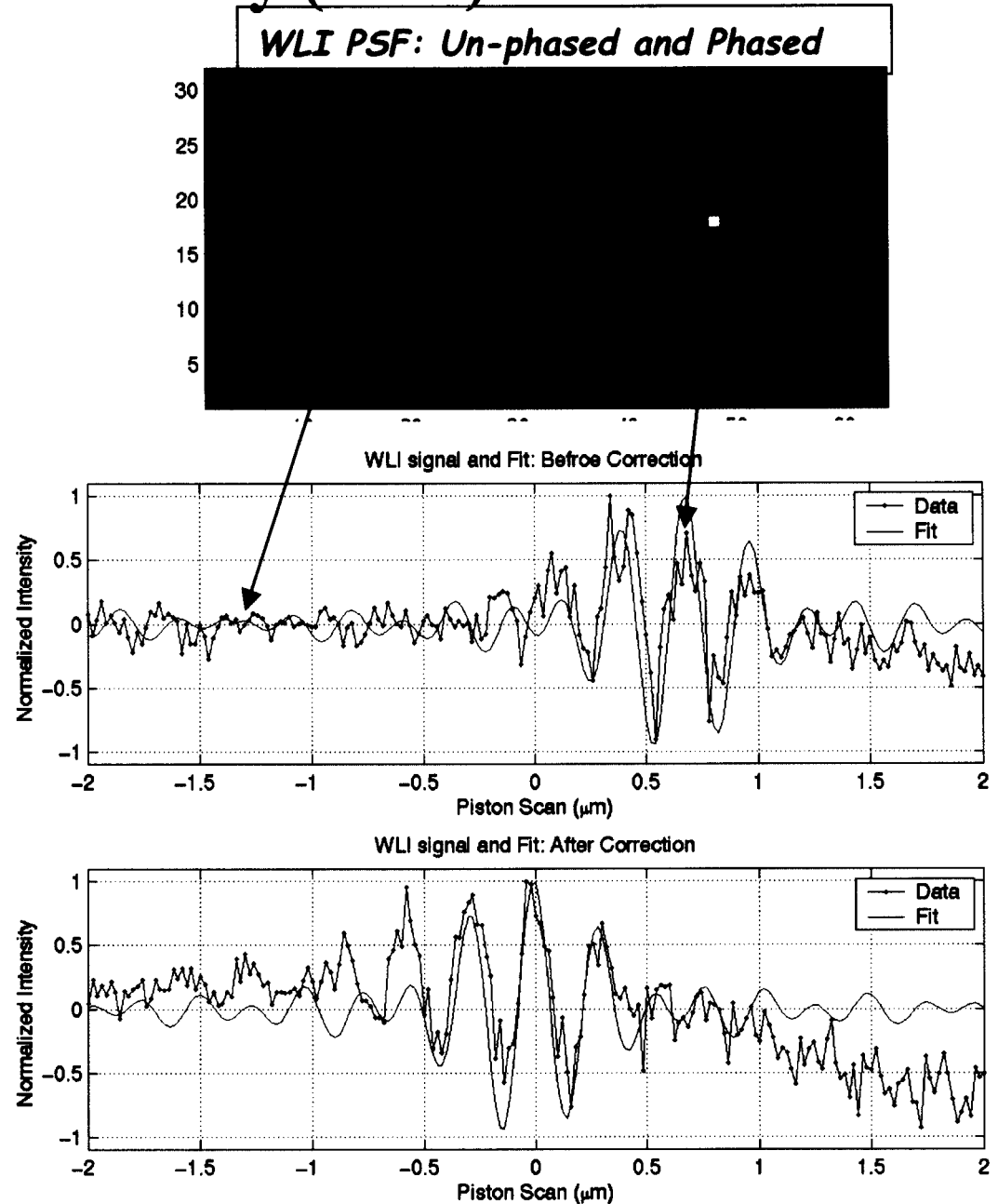


- Processed fringes after implementing correction show very little modulation
 - Modulation goes to 0 when segments are phased
 - Control has achieved sub- λ residual piston error

Detected piston reduced to near zero

White Light Interferometry (WLI) on WCT-2

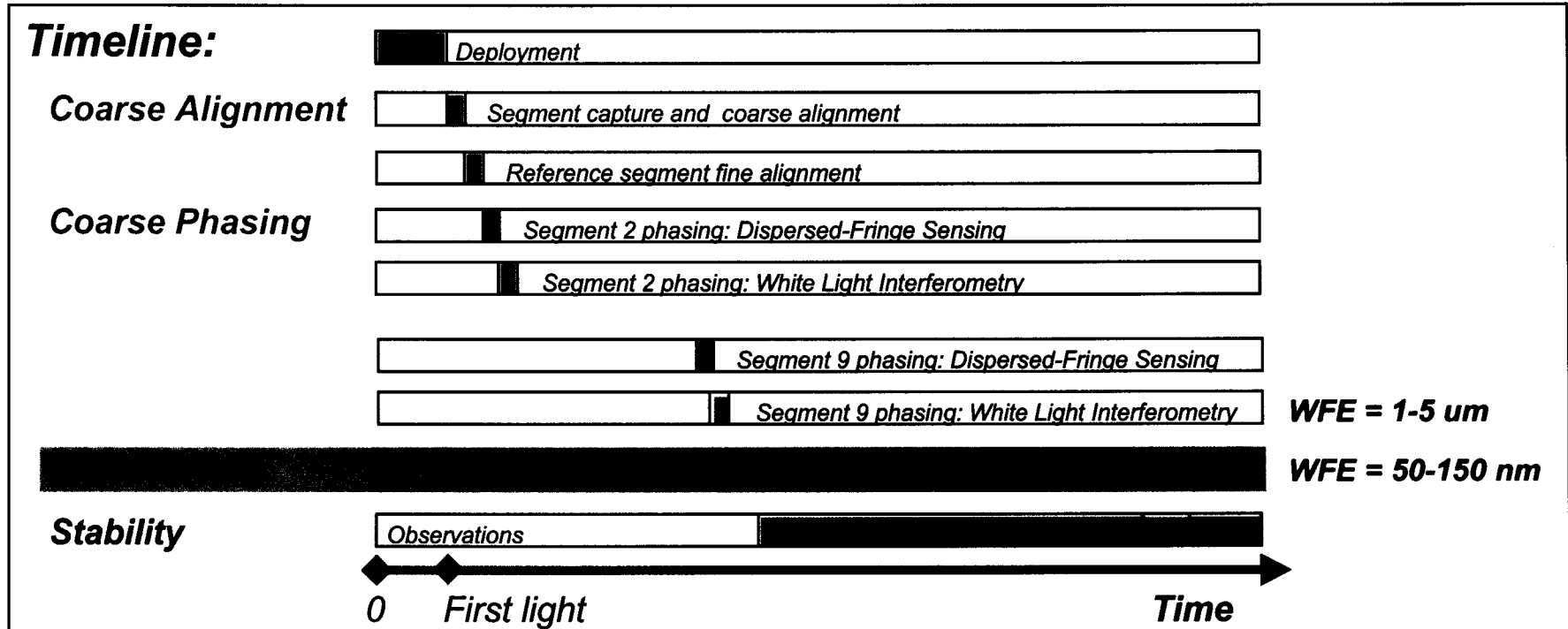
- WLI scans one segment in piston, using relative to another segment or segments, while observing in broad-band light
- Peak occurs when segments are phased, secondary peaks occur as $\delta = 2n\lambda_{\text{center}}$
- Plots show the WLI signal and its fit before and after the correction of Seg #1 relative to Seg #3 (reference), while Seg #2 is tilted away
- Piston error before correction was $-0.68 \mu\text{m}$
- After correction WLI detected $0.0 \mu\text{m}$ piston
- Independent check using IPO measured 13 nm residual piston
- WLI detection error is dominated by 20 nm scan step size
- Other error sources include image under-sampling, lab seeing, and jitter



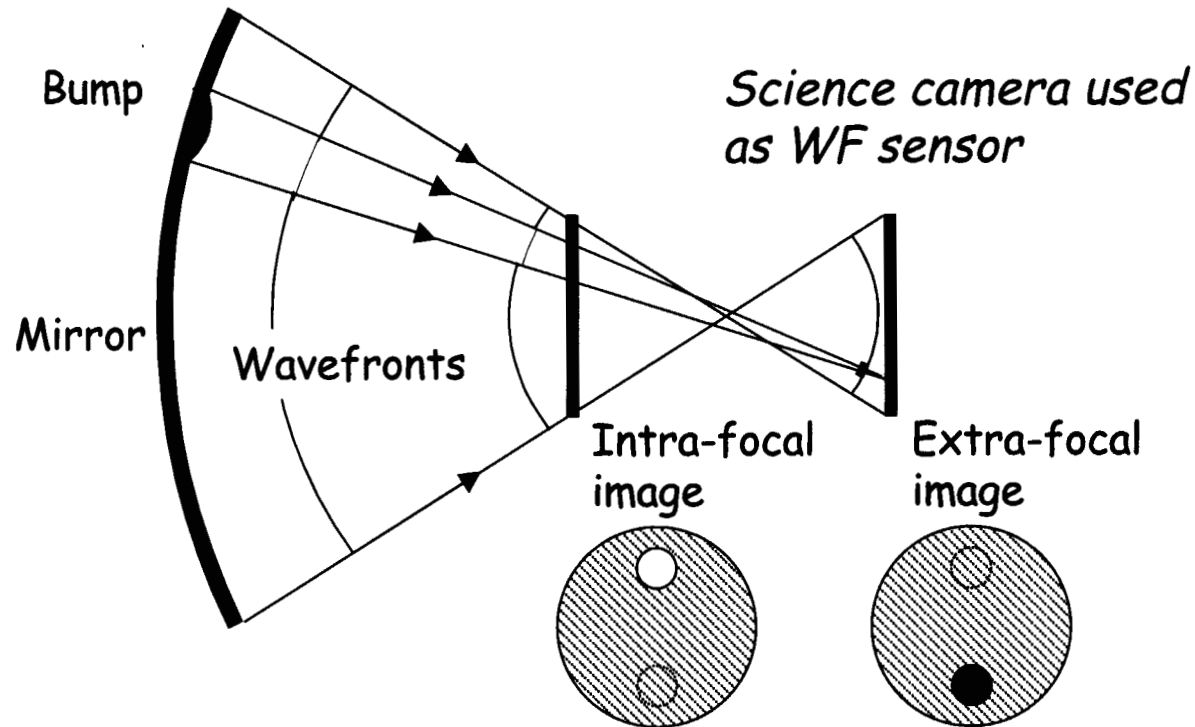
Coarse Alignment and Coarse Phasing Summary

- WCT-2 performance exceeds requirements and expectations
- Coarse alignment segment capture exceeds expected misalignments
 - Focusing algorithm -- camera stage test:
 - Before: > 10 mm (limited by camera FOV chosen)
 - After: < depth of focus (± 0.35 mm @ 633 nm)
- Segment mirror tilt errors:
 - Before: > 0.6 mrad (limited by segment actuator stroke)
 - After: < 4 μ rad (limited by the jitter & seeing)
- Segment mirror piston errors:
 - Before: $\sim 10 - 20$ μ m (limited by segment actuator stroke)
 - After: < 0.1 μ m (DFS) (confirmed by PR and IPO)
 - < 0.02 μ m (WLI) (confirmed by PR and IPO)

Fine Phasing

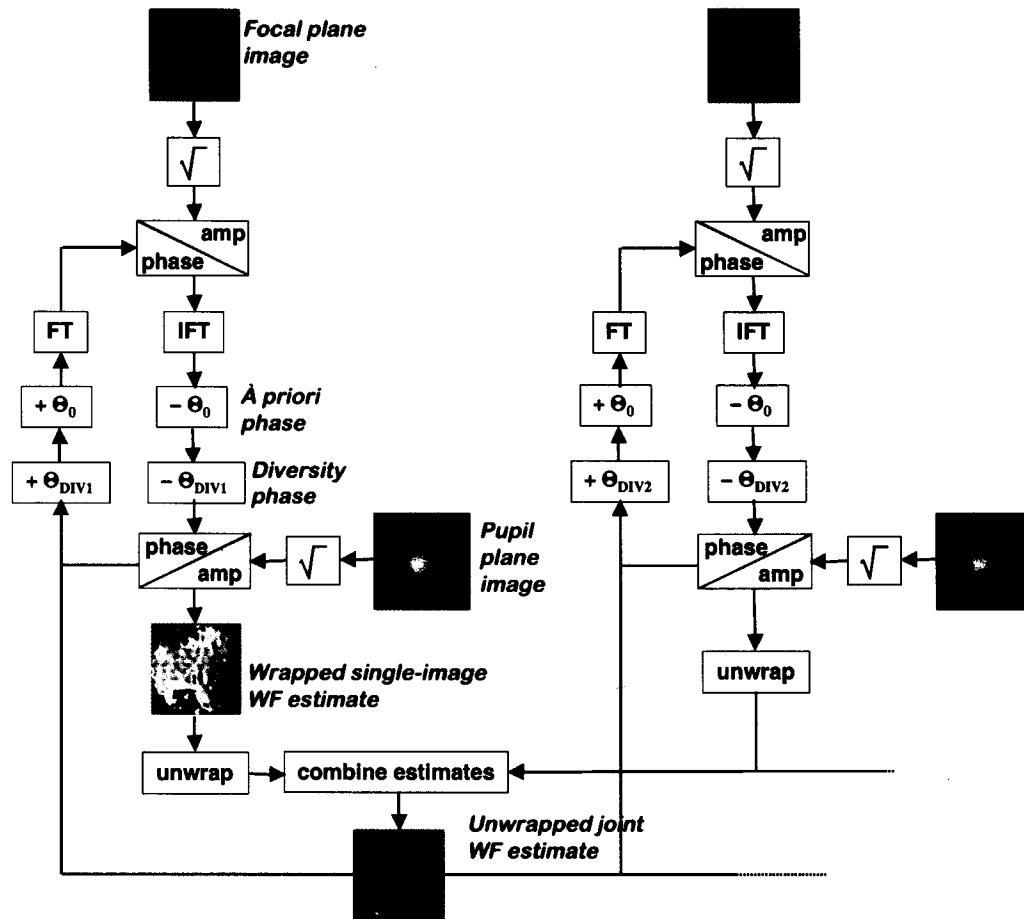


WF Sensing Using Images



- A bump on the mirror surface shifts the focus of a patch of the beam
- This shows up as a bright spot on one side of focus and a dark spot on the other
- Computer processing of multiple defocussed images correlates the intensity variations in each, derives common WF phase map
- This phase map is then used to compute new control settings

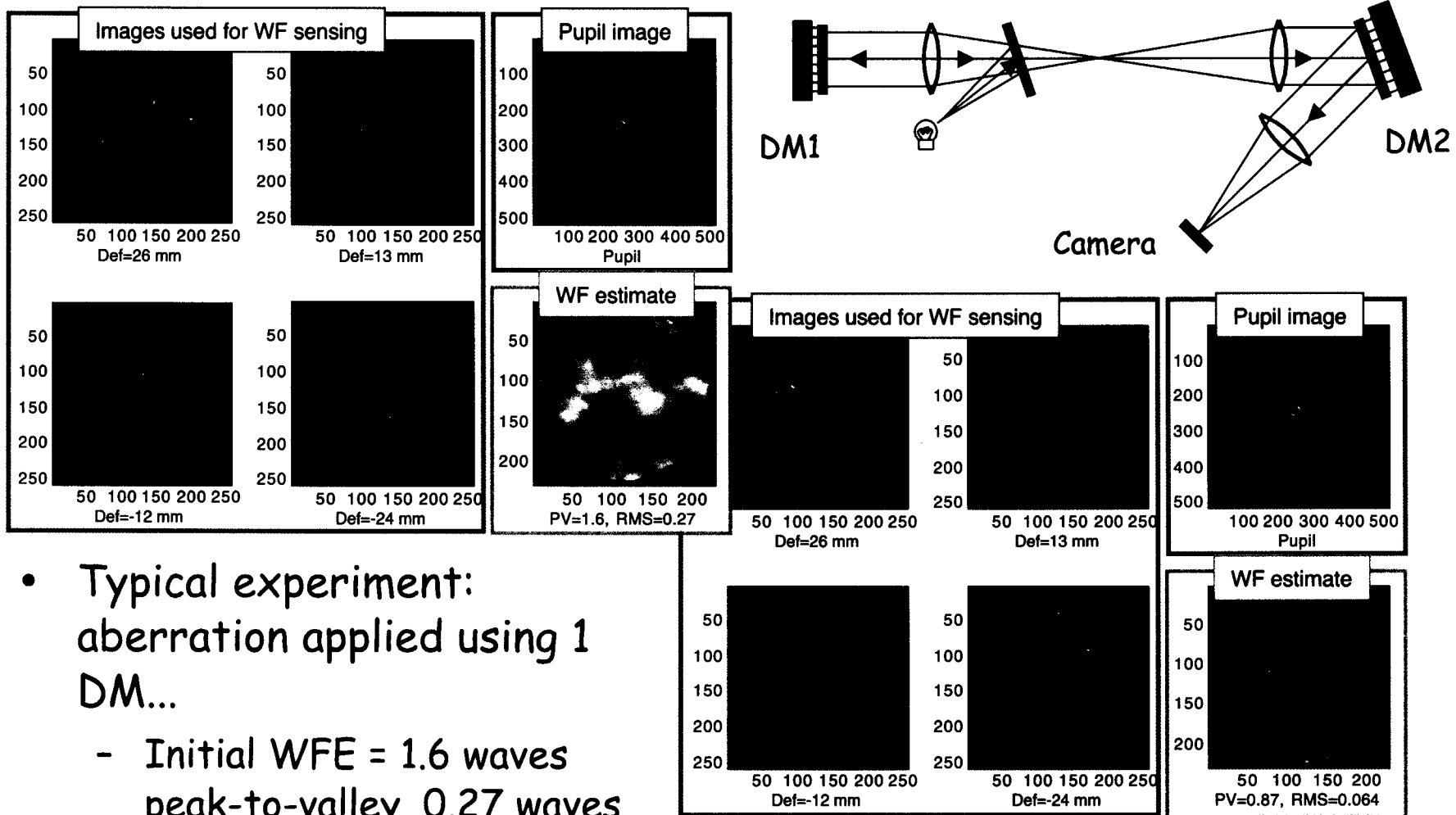
Modified Gerchberg-Saxton Algorithm



- Uses pupil image data to halve number of unknowns
- Uses defocussed images to improve visibility of aberrations
 - Reduces contrast between low, high- f effects
 - Reduces impact of jitter, other blurring
- Subtracts known phase (θ_0, θ_{DIV}) from the iteration to reduce iteration dynamic range

- Uses multiple images overdetermine solution to ensure uniqueness
 - Provides more data without introducing new unknowns
- Phase unwrapping allows estimation of WFE $> \lambda$
 - Joint unwrapping improves unwrapping robustness

Example from NGST WFC Testbed

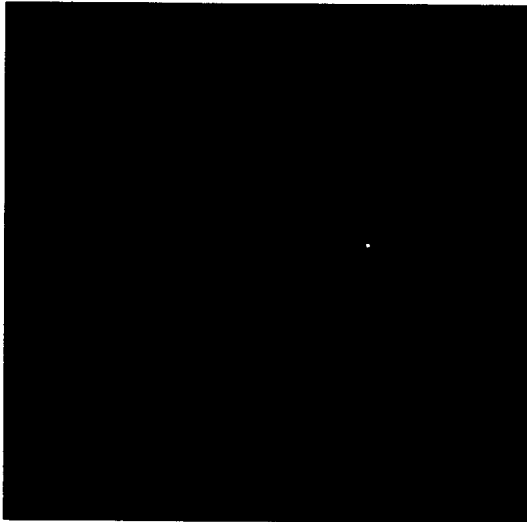


- Typical experiment:
aberration applied using 1 DM...
 - Initial WFE = 1.6 waves
peak-to-valley, 0.27 waves
RMS

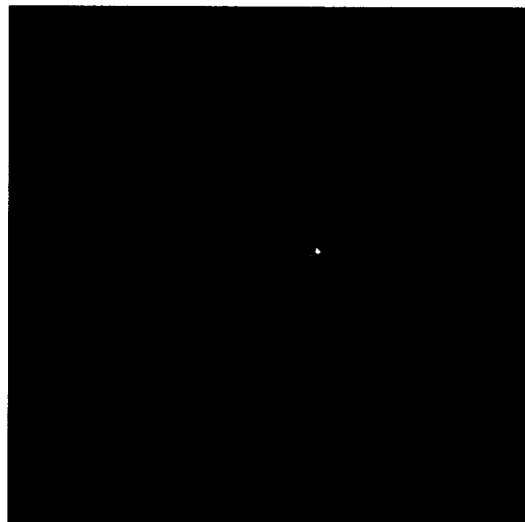
- ... and corrected using second DM
 - After control WFE = 0.87 waves
PV, 0.064 waves RMS

WCT-2 Phase Retrieval Example

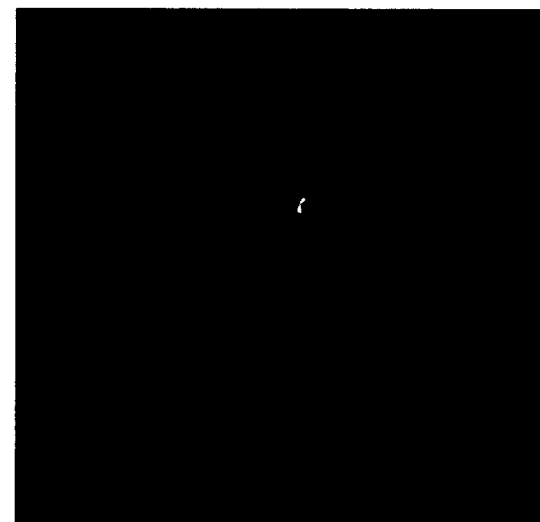
defocus = 25 mm



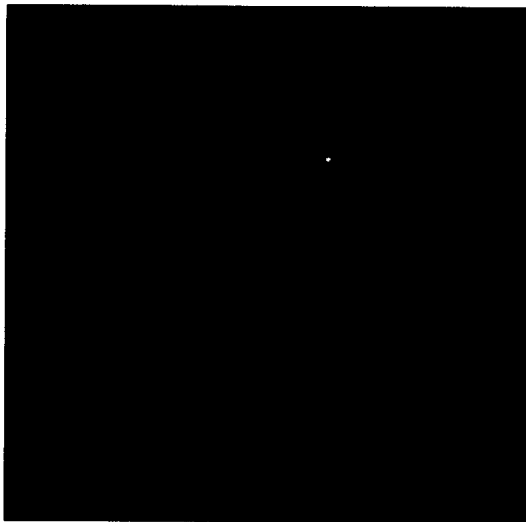
defocus = 12.5 mm



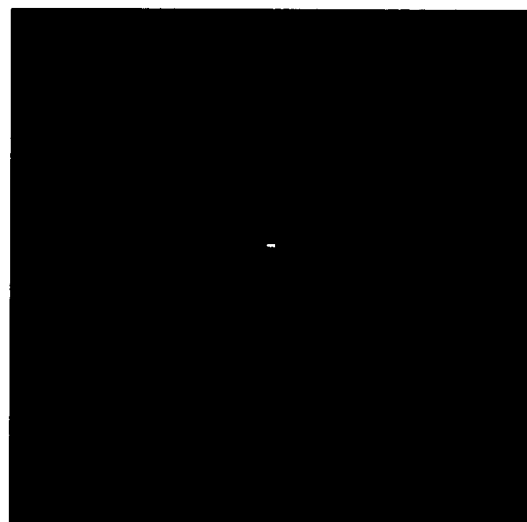
defocus = -12.5 mm



defocus = -25 mm



defocus = 0.8 mm



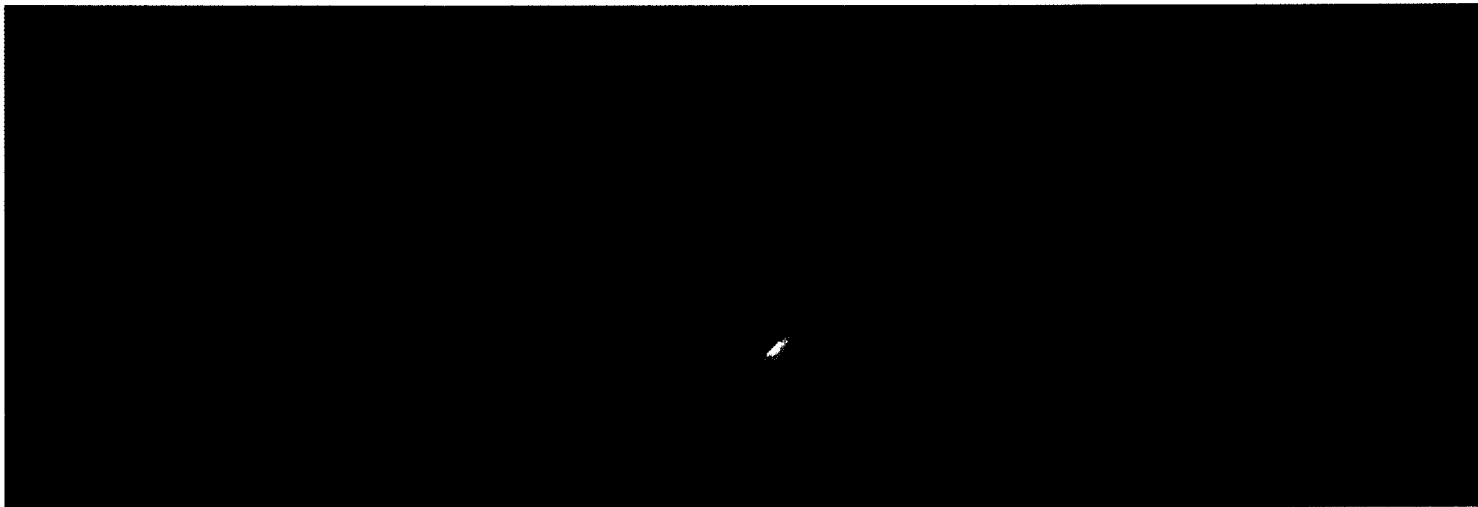
estimate



RMS = 0.237 waves

P-V = 1.11 waves

WCT-2 Segment Piston Example

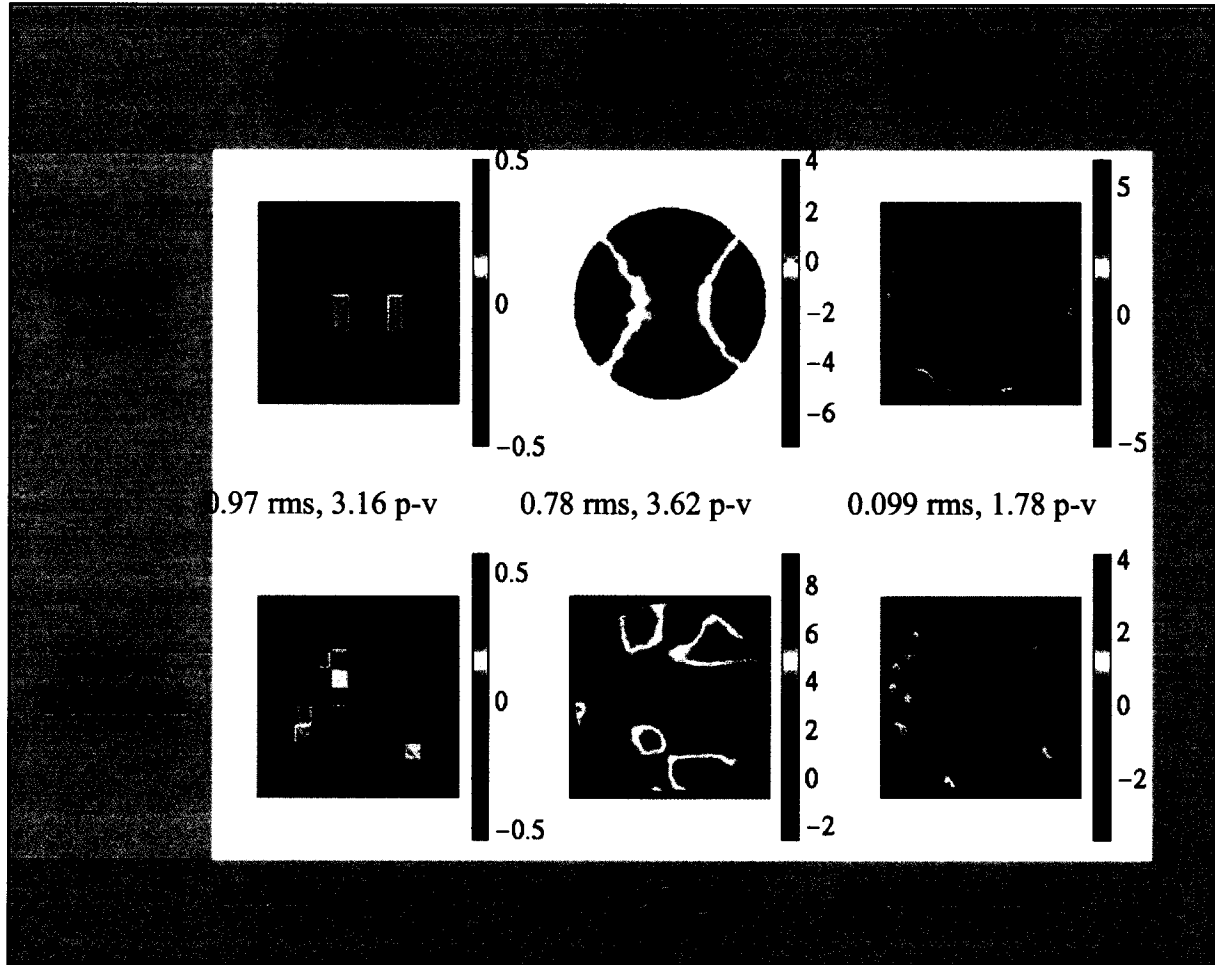
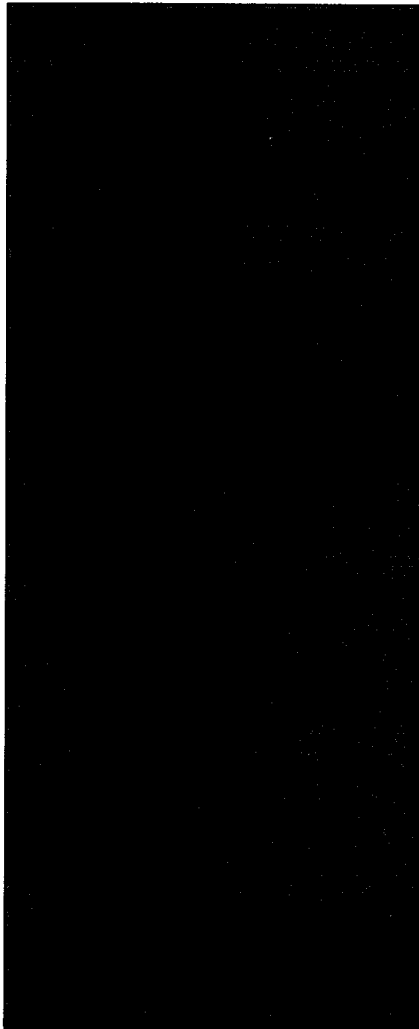


initial

piston segment 3

difference

High Dynamic Range Retrieval & Control Examples

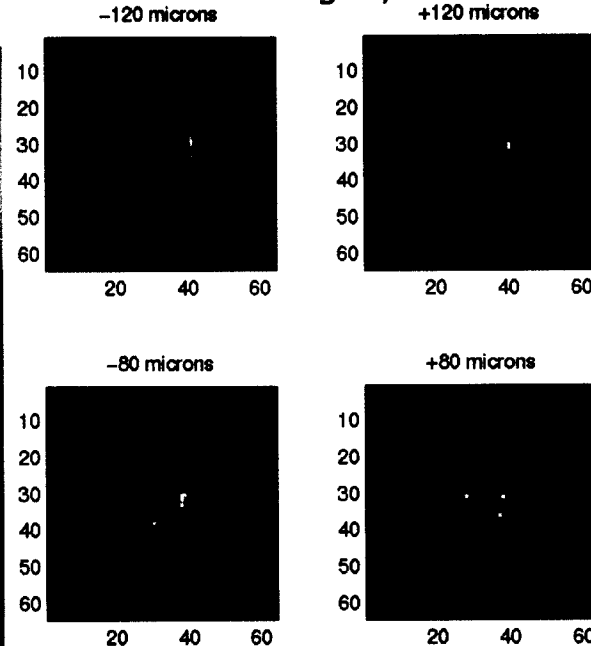


SIRTF Brutus Test

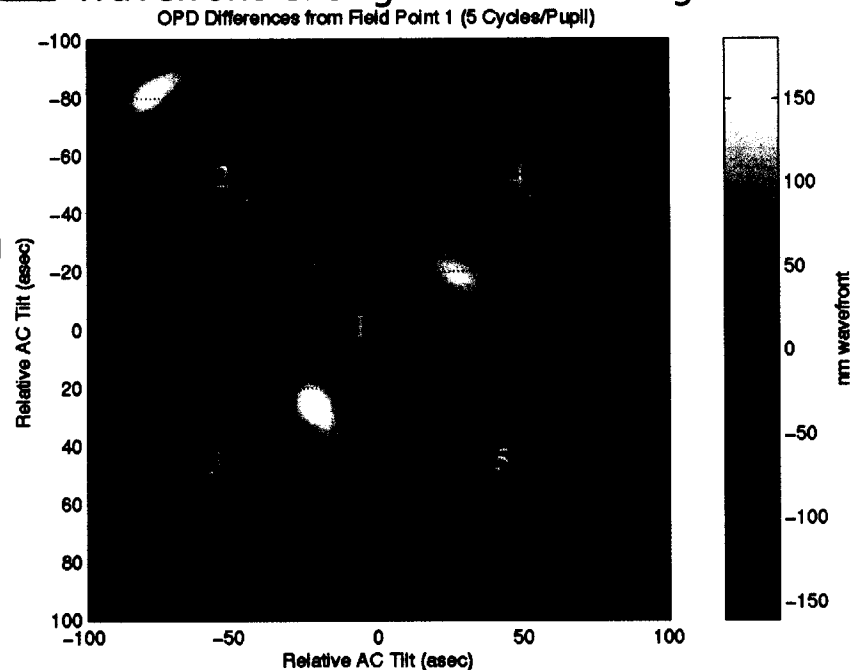
Telescope set up
for vibe test



Defocussed Images, Field Pt. 1

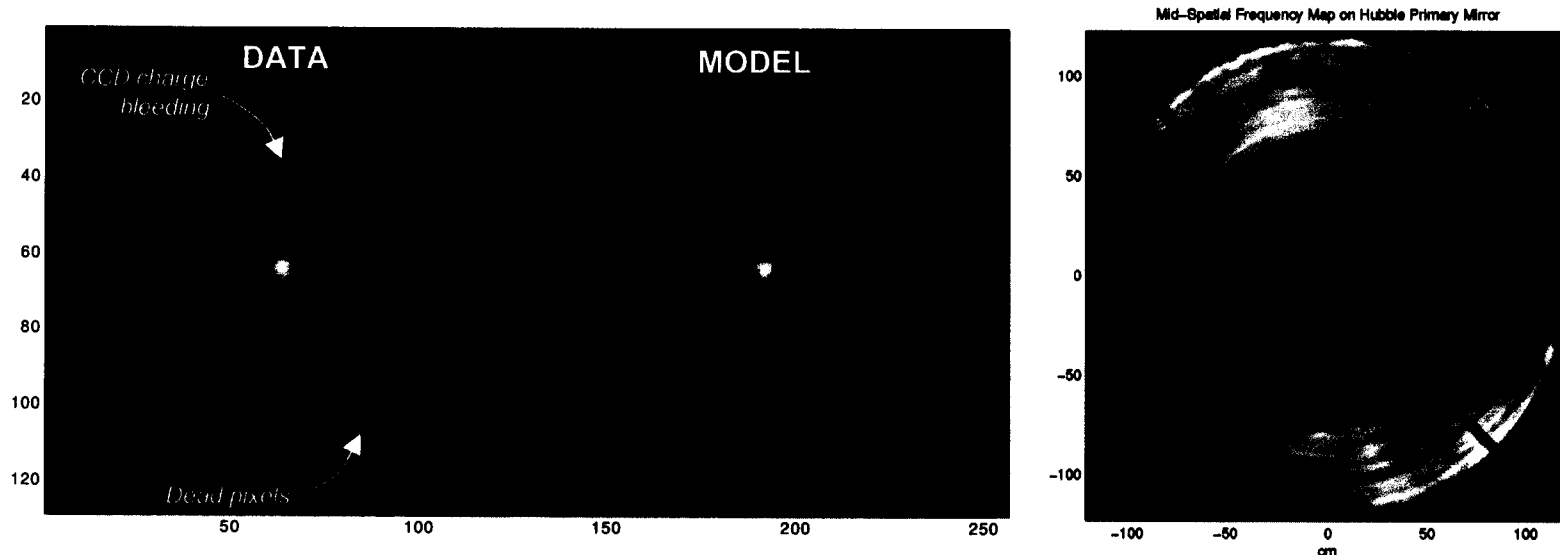


Wavefront Change with Field Angle



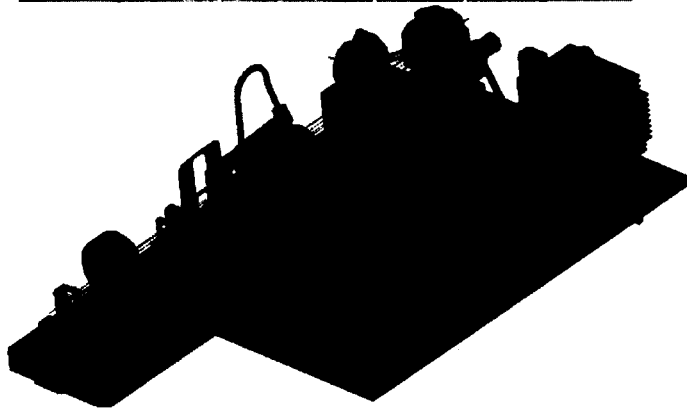
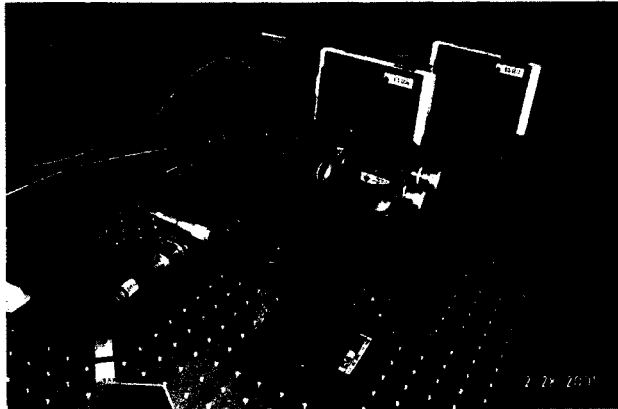
- SIRTF telescope end-to-end cryogenic optical test
 - Internal light source and autocollimating flat provide for in-chamber test capability
- Image-based WF sensing successfully measured WF at multiple field points
- Attempt to separate autocollimator bending from telescope focus shift was inconclusive
 - High degree of correlation measured between these components, even with field diversity
 - Focus was set using direct measurements

Image-Based WF Sensing Heritage Includes Hubble Space Telescope

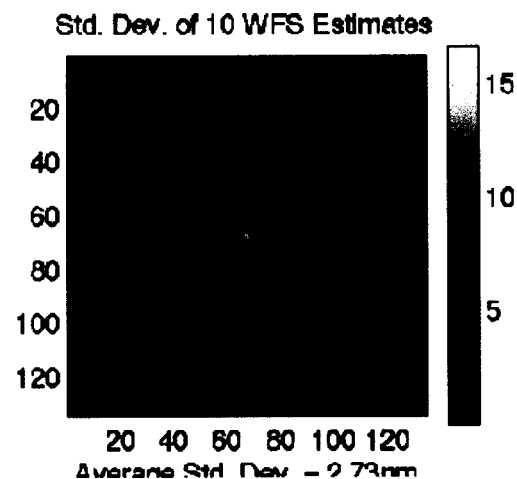
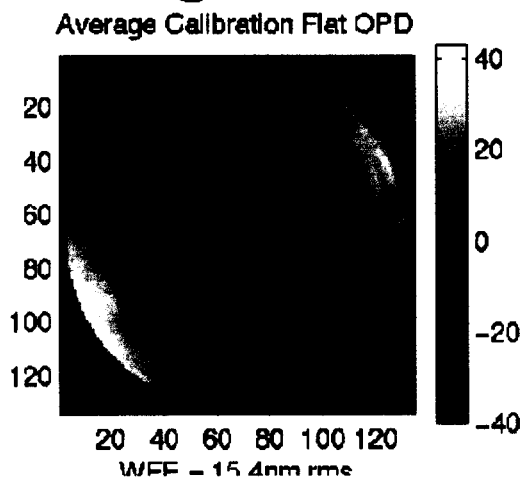


- "DATA" image is a composite of three exposures of star Feige 23, taken Oct 24, 1998 as a calibration image, displayed with a log10 stretch
 - Exposure times of 1, 4, 100 seconds provide high dynamic range
 - Taken with PC1 camera, F606W filter
- "MODEL" image is computed using HST model incorporating retrieved high-resolution mirror map
 - Map estimated using WF sensing operating on archival data
 - Model further optimized to match this image using prescription retrieval
 - From P. Dumont, D. Redding, S. Love, S. Basinger, R. Hanisch, J. Mo, "High Fidelity HST/WFPC-2 PSFs, Method and Results," JPL Report (2001).

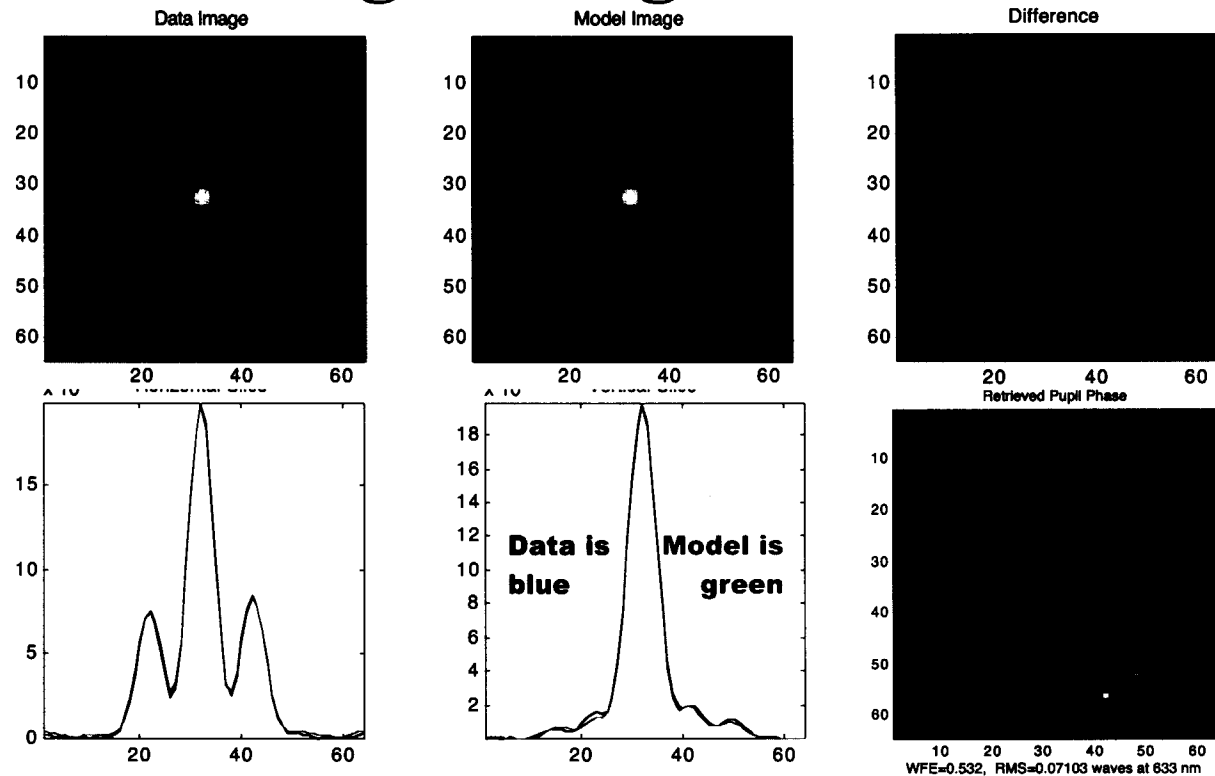
Phase Retrieval Camera (PRC)



- An imaging camera for WF sensing
 - Provides a "portable WFC testbed" for use with NMSD, AMSD, other optics
 - Provides large optics WFC experience before NAR
- Calibrated performance (using internal calibration flat on flip stage)
 - 15.4 nm static WF aberration
 - 1/325 wave repeatability for low spatial frequency WF errors
 - Performance verified by comparison with Zygo interferometer

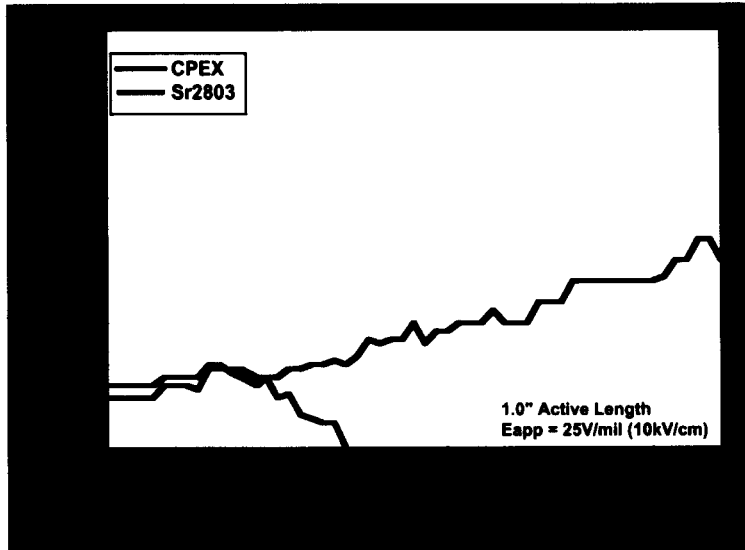


PSF Monitoring During Science

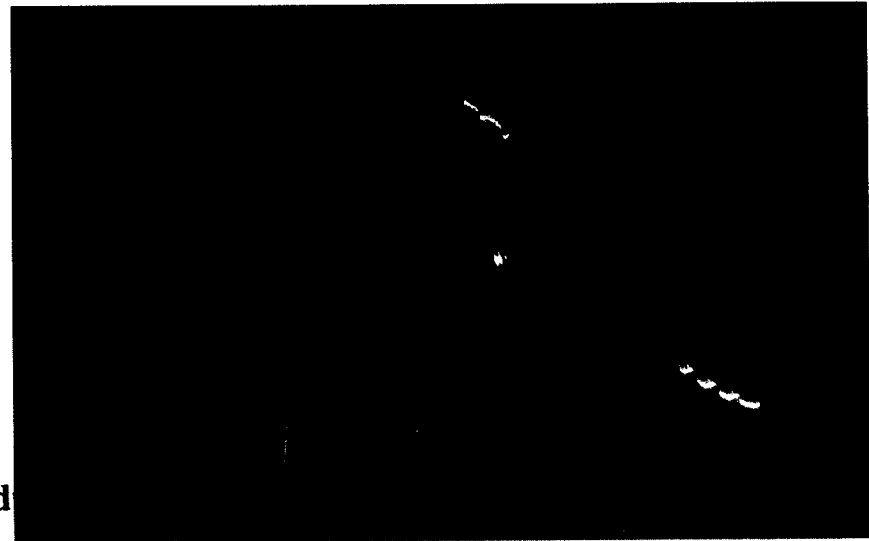


- "Infocus PSF Optimizer" (IPO) estimates WF from infocus imagery
- Experiments using WCT-2 show robust, accurate low spatial-frequency WF control
 - Measure and control tip-tilt-piston for 3 segments
 - Sensing range of $\lambda/2$, accuracy of $\lambda/100$ demonstrated
- Simulations using more complex 9- and 36-segment NGST models show good performance monitoring PSF quality

Cryogenic Deformable Mirror Technology



Mod



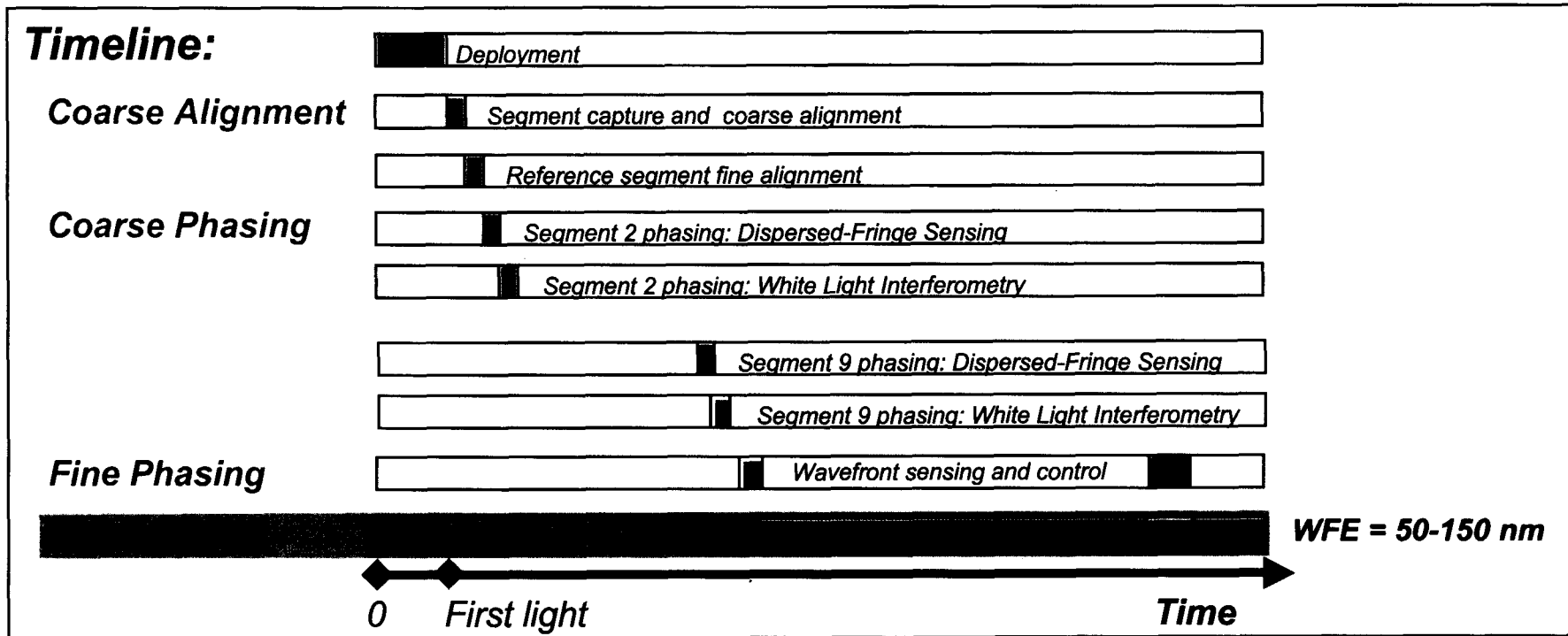
Cryoceramic materials for DM actuators meet stroke objectives over NGST operational temperature range



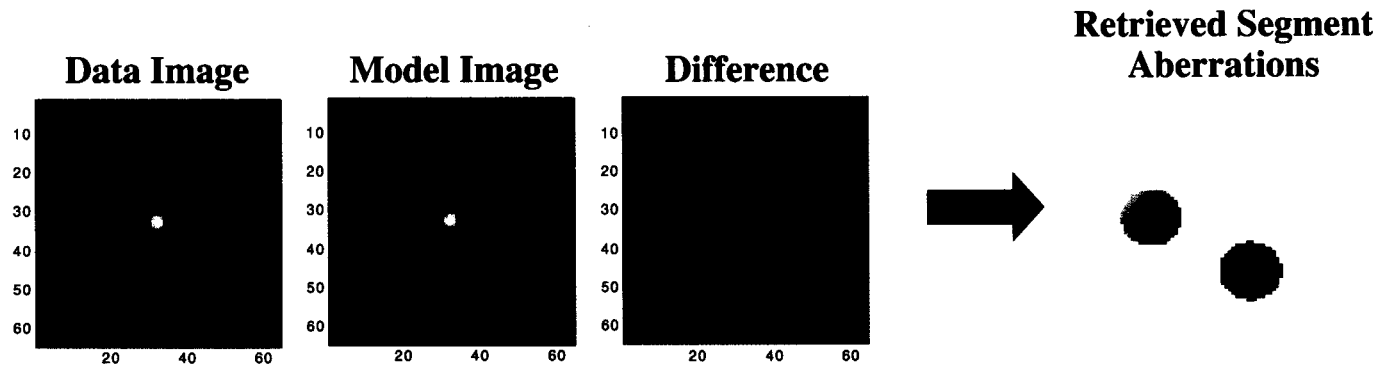
Modular actuator array with integrated electrical connections provides better performance, lower risk for cryo DM



Maintenance: PSF Monitoring and/or Metrology

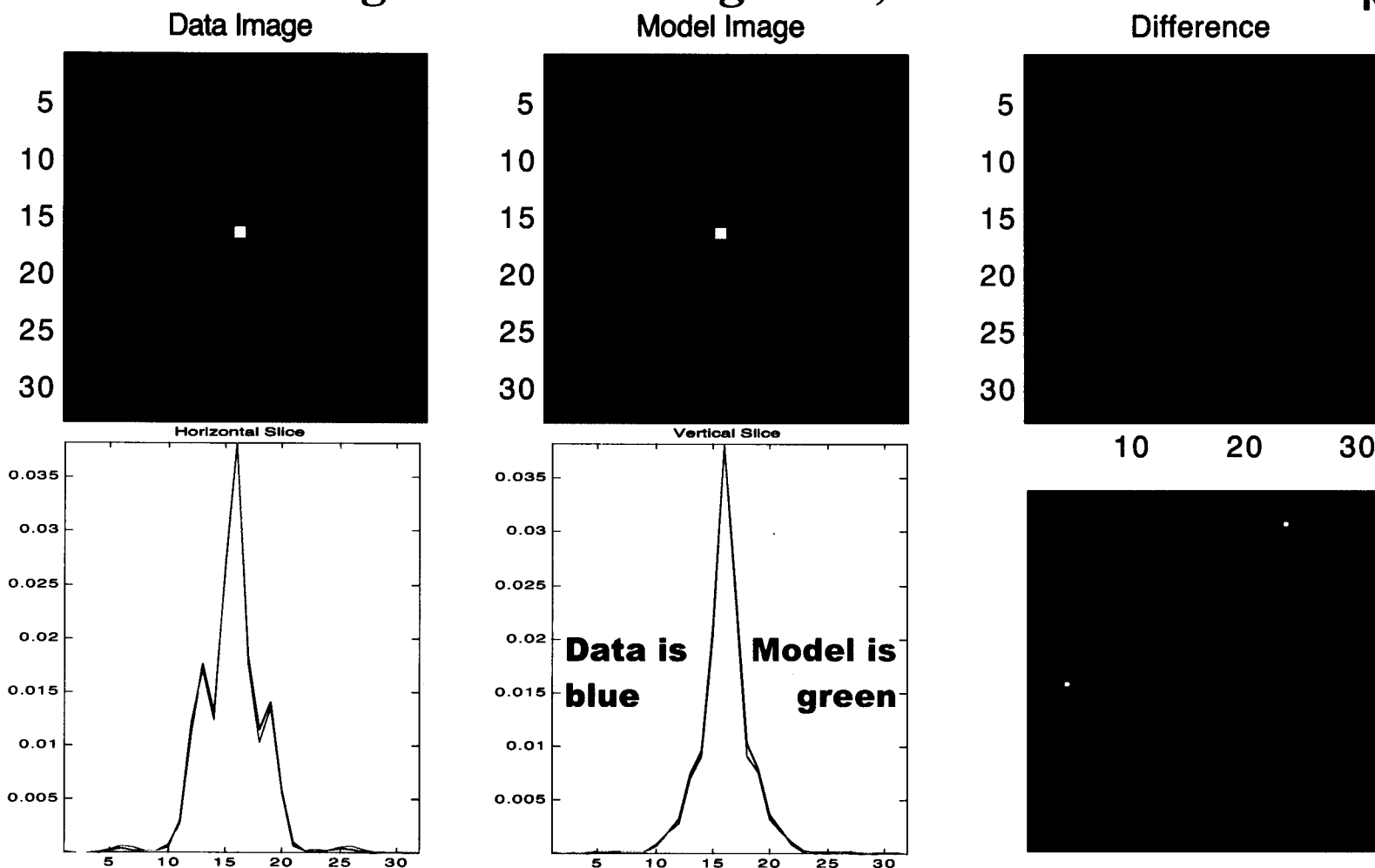


In-focus PSF Optimizer (IPO)



- IPO uses in-focus images to measure low-order WF aberrations
 - "Prescription retrieval:" optimization function (Levenberg-Marquardt method) drives model parameters to match simulated images to data.
 - ◆ WCT-2 model includes segment piston, tip/tilt
 - ◆ Model can also include high resolution prior terms from other WFS and modeling sources.
 - ◆ Retrieved parameters are used to determine necessary controls

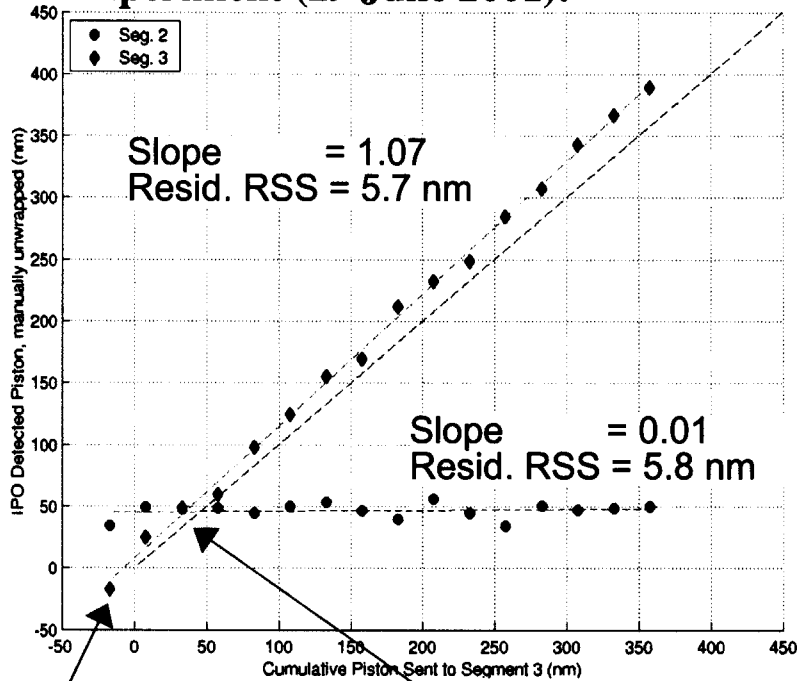
Infocus Image: No PSF Magnifier, $\lambda = 900$ nm



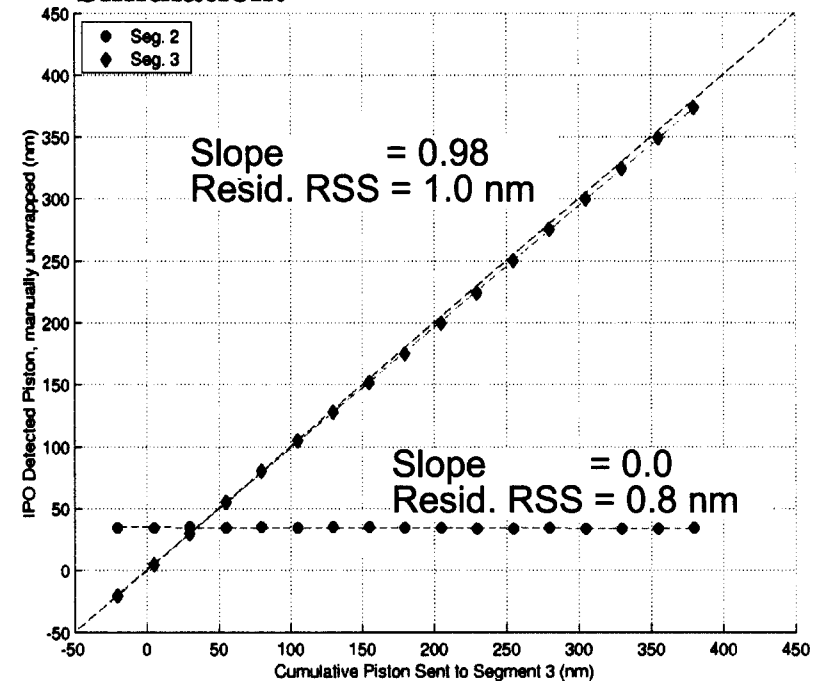
- WCT-2 data
 - 900 nm filter
 - 0.1 sec exposure time for min jitter
 - 250 frames
 - Subpixel shift-and-add
- Frame selection
- No PSF magnifier
- Blur half-width = 0.54 pixels
- Match = 0.026 RSS vs. total of 25

Piston Accuracy with PSF Magnifier ($\lambda=900$ nm)

Experiment (29 June 2001):

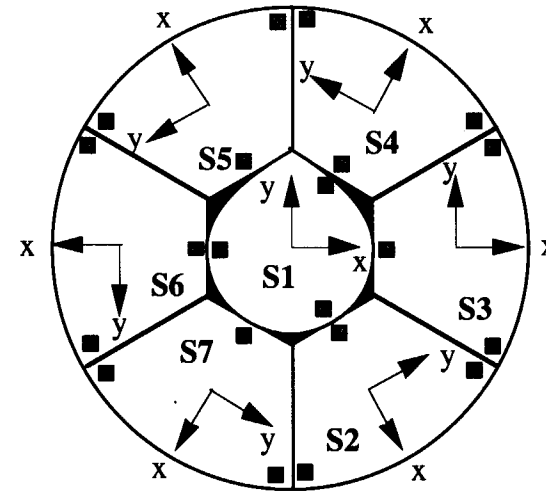
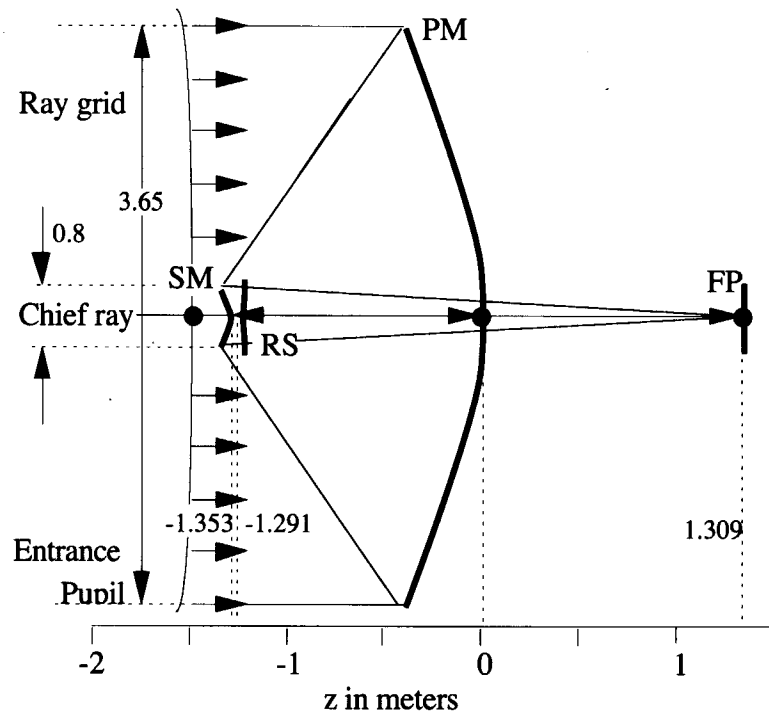


Simulation:



- Piston Seg. 3 in steps of +25 nm. Detected piston was manually unwrapped after 225 nm ($\lambda/4$).
- Residual errors show ~ 6 nm piston detection uncertainty (RSS), which is on the same order as the 5 nm PZT

Control of Segmented PM using Metrology



- A submm space telescope problem: keep good WF quality using metrology only (edge sensors, laser gauges)

WF Estimator

- Estimator objective:

$$J = \frac{1}{2} [\vec{x}_0^T \mathbf{X}_0^{-1} \vec{x}_0 + (\vec{z} - \mathbf{H}\vec{x}_0)^T \mathbf{R}^{-1} (\vec{z} - \mathbf{H}\vec{x}_0)]$$

$$dJ = d\vec{x}_0^T [\mathbf{X}_0^{-1} \vec{x}_0 - \mathbf{H}^T \mathbf{R}^{-1} (\vec{z} - \mathbf{H}\vec{x}_0)] = 0$$

- Solution:

$$\vec{x}_{\text{est}} = \mathbf{K}\mathbf{H}\vec{x}_0 + \mathbf{K}\vec{r}$$

$$\mathbf{K} = \mathbf{P}^{-1} \mathbf{H}^T \mathbf{R}^{-1}$$

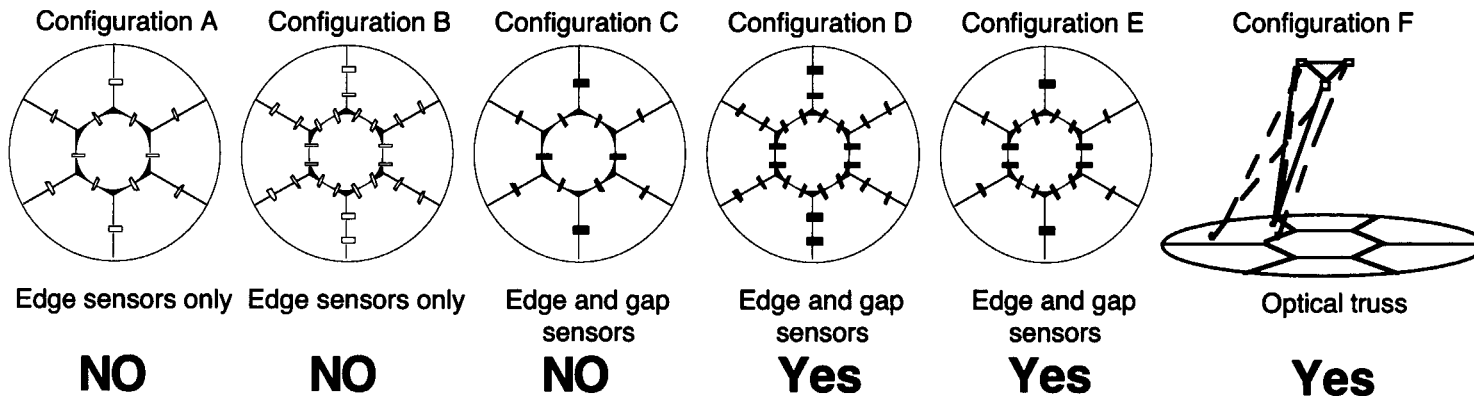
$$\mathbf{P}^{-1} = \mathbf{X}_0^{-1} - \mathbf{H}^T \mathbf{R}^{-1} \mathbf{H}$$

- Error:

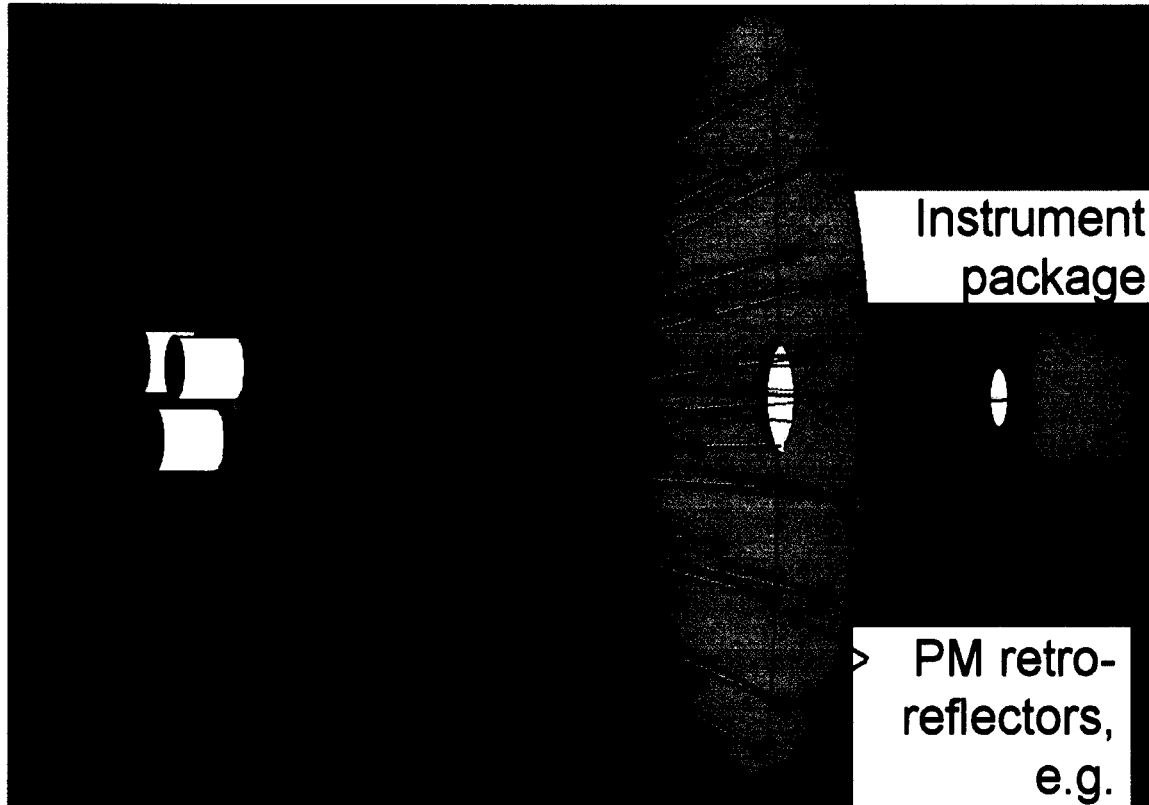
$$\vec{e}_x = \vec{x}_0 - \vec{x}_{\text{est}} = (\mathbf{I} - \mathbf{K}\mathbf{H})\vec{x}_0 - \mathbf{K}\vec{r}$$

$$\mathbf{E} = (\mathbf{I} - \mathbf{K}\mathbf{H})\mathbf{X}_0(\mathbf{I} - \mathbf{K}\mathbf{H})^T - \mathbf{K}\mathbf{R}\mathbf{K}^T = (\mathbf{I} - \mathbf{K}\mathbf{H})\mathbf{X}_0 = \mathbf{P}$$

Does Sensor Configuration Observe Wavefront Errors?



Laser Truss Application of SIM Metrology



Laser truss can fully measure motions that affect optical quality

3 retroreflectors per segment for rigid-body motions, more for flex deformations

Absolute mode for large dynamic range, low accuracy

Relative mode for high accuracy

Optical fiber couples laser on warm side to cold beam launcher

Other configurations may be useful (backside of PM, for instance)

COPHI demonstrated performance in relative mode:

<u>Sensing bandwidth</u>	<u>1 Hz</u>	<u>100 Hz</u>	<u>10 kHz</u>
Resolution	0.005 nm	0.02 nm	0.1 nm
Thermal Stability	Better than 1 nm/K		

WFC Technology Heritage Matrix

Approximate Technology Readiness Levels (TRLs) for Cryo SubMM/FIR missions

<u>Control Mode</u>	<u>NGST</u>	<u>PSR</u>	<u>SIM</u>	<u>SIRTF</u>	<u>Other</u>
Capture	TRL4	TRL2			
Coarse Alignment	TRL4	TRL2			
Coarse Phasing					
White-Light Interferometry (WLI)	TRL4				TRL2?
Dispersed-Fringe Sensor (DFS)	TRL4				
Keck Phasing Camera					TRL2?
Fine Phasing					
Image-based WFS	TRL4			TRL5	
Dedicated WFS					TRL2?
Maintenance					
Edge sensing systems		TRL2			???
Laser truss metrology		TRL2	TRL4?		
Cryogenic components					
Segment actuators	TRL5?				
DM actuators	TRL				
Cryo edge/gap sensors		TRL2			???